Electronic Supplementary Material (ESI) for Journal of Materials Chemistry C.

Supporting Information

Interfacial Doping of Semiconducting Polymers with Phenothiazine-based Polymeric Ionic Liquids

Saejin Oh,[a] Phong H. Nguyen,[b] Thi M. Tran,[a] Audra J. DeStefano,[b] Kan Tagami,[a] Dafei Yuan[c], Andrei Nikolaev,[a] Marcus Condarcure,[b] Songi Han,[a,b] Javier Read de Alaniz,[a] and Michael L. Chabinyc[d*]*

[a]Department of Chemistry and Biochemistry, [b]Department of Chemical Engineering, [c]Mitsubishi Center for Advanced Materials, University of California, Santa Barbara, CA, 93106–5050, USA, [d]Materials Department, University of California, Santa Barbara, California 93106, United States

*Email addresses of corresponding authors:

Michael L. Chabinyc: mchabinyc@engineering.ucsb.edu

Javier Read de Alaniz: javier@chem.ucsb.edu

Materials. P3HT (Lisicon, SP001) was purchased from Merck. $NOPF_6$, NaTFSI and anhydrous dichlorobenzene (CB)/dichloromethane (DCM) were purchased from Sigma-Aldrich. All are used without further purification.

Synthesis of PTZ-EE monomer. Intermediate products were prepared using the same procedures from our previous work.[1] We observed the limitation of the last Wittig step to synthesize the final monomer (i.e., small scale). To gain more material for the interfacial doping studies, the scale-up synthetic step to form PTZ-EE monomer was optimized as below.

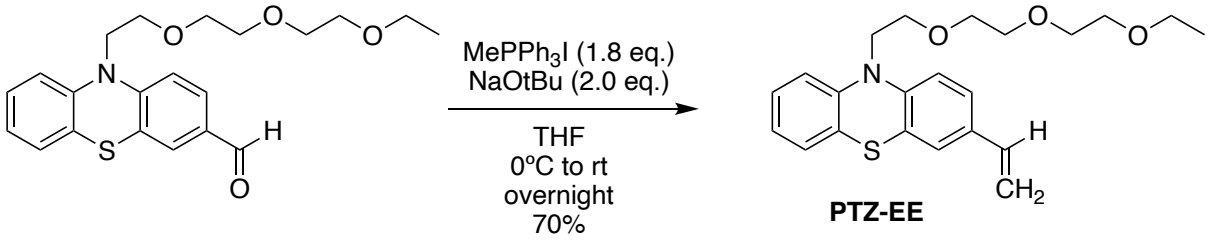

To a flame-dried round-bottomed flask equipped with a stir bar was added methyltriphenylphosphonium iodide (13.33 g, 32.98 mmol, 1.80 equiv.) and sodium *tert*-butoxide (3.52 g, 36.65 mmol, 2.00 equiv.) in freshly distilled THF at 0 °C. The mixture was stirred for 40 min at room temperature. A solution of the aldehyde starting material (7.1 g, 18.32 mmol, 1.00 equiv.) in freshly distilled THF was then added at 0 °C. The reaction was allowed to warm up to room temperature and stirred for 24 hours. Upon completion, the reaction was quenched with deionized water and extracted with DCM (x3). The organic phase was dried with Na_2SO_4, and concentrated in vacuo. The crude product was purified by flash column chromatography, eluting with 30% ethyl acetate in hexanes and furnished the pure product **PTZ-EE** (5.00 g, 12.97 mmol) in 70% isolated yield.

Synthesis of pPTZ-EE. To a flame-dried 2-neck round bottom flask, equipped with a stir bar, was added PTH monomer (800 mg, 2.0 mmol, 1.0 eq.), fresh AIBN (1.6 mg, 0.0098 mmol, 0.5 mol%), and TEMPO (3 mg, 0.020 mmol, 1 mol%). One neck of the flask was equipped with a reflux condenser. The mixture was sparged with nitrogen for 30 min to remove residual oxigen. The mixture was then heated neat at 125 °C for 24 h under nitrogen. The crude polymer was precipitated in cold MeOH three times to afford the pure yellow-oil polymer (550 mg, PDI = 2.0, and Mn = 22 kDa). Doped pPTZ-EE were synthesized and characterized based on the procedures reported in the previous work[1]. The result on the ion exchange and the actual radical counts were also performed as described in the previous literature.[1]

Polymer thin films fabrication. The quartz or Si wafer substrates were cleaned with detergent, deionized water, acetone, and isopropyl alcohol prior to spin coating. Pristine P3HT solution was prepared with 10 mg/mL concentration with CB and stirred at 80 °C for 12 hours. Then, the pristine P3HT thin films were fabricated by spin coating the 100 μL solution on the substrate with 1000 rpm/45 sec/500 acc, followed by 3000 rpm/30 sec/3000 acc. Then, P3HT thin films are thermally annealed at 130 °C for 30 min.

For P3HT/pPTZ-EE bilayers, 5 mg/mL partially doped pPTZ-EE/TFSI solutions in DCM were prepared at room temperature, and spun-cast on top of the pristine P3HT thin films, with 1000 rpm/30 sec/500 acc. Instant color change from deep purple to lighter purple was observed after bilayer formation. Film thicknesses were measured by Bruker DektakXT Stylus profilometer.

Continuous Wave Electron Paramagnetic Resonance (cw-EPR) Spectroscopy. Spin concentrations are determined from cw-EPR spectra using a calibration curve of TEMPO in dichloromethane. All spectra are acquired on a Bruker EMX spectrometer equipped with a dielectric cavity (Bruker ER 4123) and an ER041 MR microwave bridge. Samples are loaded into a 0.8 millimeter ID quartz capillary and sealed on both sides with wax. Capillaries are then placed in a 3 millimeter ID quartz EPR tube and inserted into the cavity. Instrument parameters include a microwave power of 1.9 milliwatts, modulation amplitude of 1 gauss, and a modulation frequency of 100 kilohertz.

UV-vis-NIR Spectroscopy. UV-vis-NIR spectra was acquired using Shimadzu UV3600 UV-Nir-NIR spectrometer. For P3HT solution sample, chlorobenzene (CB) was used as the solvent, and the solution was prepared with 0.67 mg/mL concentration. For solid state samples, thin films were prepared on quartz substrates and placed inside the instrument for measurements. The spectra were acquired by scanning from 250 to 2500 nm, with medium scan speed.

X-ray photoelectron spectroscopy. X-ray photoelectron spectroscopy (XPS) measurements were conducted using an Escalab Xi^+ Spectrometer (ThermoFisher Scientific), employing a monochromatic aluminum Kα X-ray source under a vacuum of 10^{-8} Torr. Charge compensation was accomplished with a dual ion-electron low-energy flood source. Survey spectra were captured with a 100 eV pass energy, comprising 5 scans taken at 0.5 eV intervals with a 50 ms dwell time. Depth profiling was carried out utilizing an Ar^+ cluster gun featuring a cluster size of 1,000 atoms

and a 5 s period, which corresponds to 4 nm intervals between survey scans. The cluster gun was rastered over a 600 × 600 μm^2 square region, and photoexcited electrons were collected from the inner 400 × 400 μm^2 to selectively isolate signal from the crater centers. The resolution depth of XPS was determined by estimating the escape depth (λ) of electron in P3HT thin films, which corresponds to ~13 nm. This was extracted by assuming most of the signals (~99.3%) was acquired from 5λ, with escape depth around 2.6 nm for P3HT.[2,3]

Calculating the number density of TFSI from XPS. First, the unique fluorine signal from $TFSI^-$ counterion was used by considering each $TFSI^-$ ion has six fluorine atoms. Then, the relative stoichiometry of P3HT and $TFSI^-$ was calculated by the known atomic ratios from their chemical structures. The fluorine atomic % was normalized relative to carbon counts, assuming that part of the C1s is coming from $TFSI^-$ counterion that has two carbons and the remaining is arising from the carbons in P3HT chains. With the known atomic ratio of $TFSI^-$ relative to P3HT, the number density of $TFSI^-$ (mol TFSI/cm^3) was extracted as shown in Fig 2. As $TFSI^-$ counterions will be present in P3HT thin films to balance the positive charge induced by polaron, we assumed that the number of polarons and the $TFSI^-$ ions present as 1:1 ratio. Thus, the number density of TFSI is equal to the polaron number density present in P3HT thin films. For the calculation, P3HT density and the molecular weight of repeat unit were assumed to be 1.1 g/cm^3 and 166.28 g/mol, respectively.

Transmission line measurements. Prior to the transmission line measurements, 40 nm of gold contacts were thermally evaporated onto pristine P3HT thin films with a shadow mask, using an

Angstrom Engineering thermal evaporator. Then, the electrical conductivity was measured by Keithley 6485 picoammeter with transmission line measurements. All electrical measurements were conducted inside the glovebox with inert atmosphere.

Grazing Incidence Wide Angle X-ray Scattering (GIWAXS). X-ray scattering of pristine and doped P3HT thin films was performed at the Stanford Synchrotron Radiation Lightsource at experimental station 11-3. X-ray energy used for scattering was 12.7 keV. Angle-dependent GIWAXS scans were acquired at the range of incidence angle of 0.05° to 0.13° with increments of 0.0025° with 100 second exposures, to get depth-dependent scattering. Samples were continuously rocked in the direction perpendicular to the X-ray flux by ± 2 mm around the sample center to mitigate beam damage during the data acquisition process.

Calculating the relative equivalence of dopant and P3HT. The number of moles of $PTZ^{\bullet+}$:$TFSI^-$ has been calculated by knowing the radical concentration (from EPR spin quantification) used for sequential casting, and the solution concentration (in mg/mL) and volume used (100 μL). The number of moles of 3HT has been calculated by the known thin film geometry, with known film thickness (from profilometry) and area of the sample. Then, the relative equivalence of $PTZ^{\bullet+}$ and 3HT was compared to demonstrate the ratio between donor and acceptor.

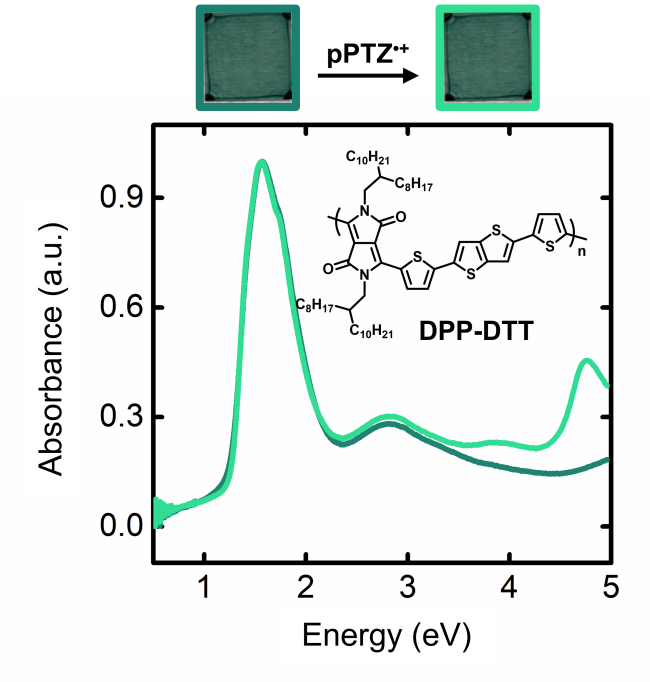

Fig S1. UV-vis-NIR spectra of pristine (black trace) and (orange trace) bilayer of DPP-DTT thin films with 26.4% doped pPTZ$^{\bullet+}$-EE/TFSI. Inset figures indicate color changes of P3HT and DPP-DTT doped with PTZ$^{\bullet+}$.

Table S1. Summary of IE and EA of electron donor and accepting materials.

Materials	IE (eV)	EA (eV)
F_4TCNQ[4,5]	-	5.2
$NOPF_6$[6,7]	-	6.5
Magic Blue[8]	-	5.8
Spiro-OMeTAD$^{\bullet+}$[9]		5.3
pPTZ-EE[1]	5.2	-
PTZ[10]	5.3	-
P3HT[4,11]	4.9/5.1	-

* The IE/EA of molecular dopants and polymers were acquired from the literature value or extracted by extrapolating the onset potential from the cyclic voltammogram. For comparison with closed shell acceptors, the EA of radical cations is determined by the reduction potential of the radical cation to neutral form.[12]

Table S2. Comparison chart of theoretical and actual % dopant loading.

TFSI loading	Theoretical % dopant loading from solid bilayer geometry	Actual % dopant loading from UV-vis	Doping efficiency from UV-vis
8.2%	**2.2**	**4.8**	**58.5%**
8.6%	**2.3**	**5.1**	**59.3%**
9.5%	**2.6**	**7.1**	**74.7%**
11.5%	**3.1**	**7.2**	**62.6%**

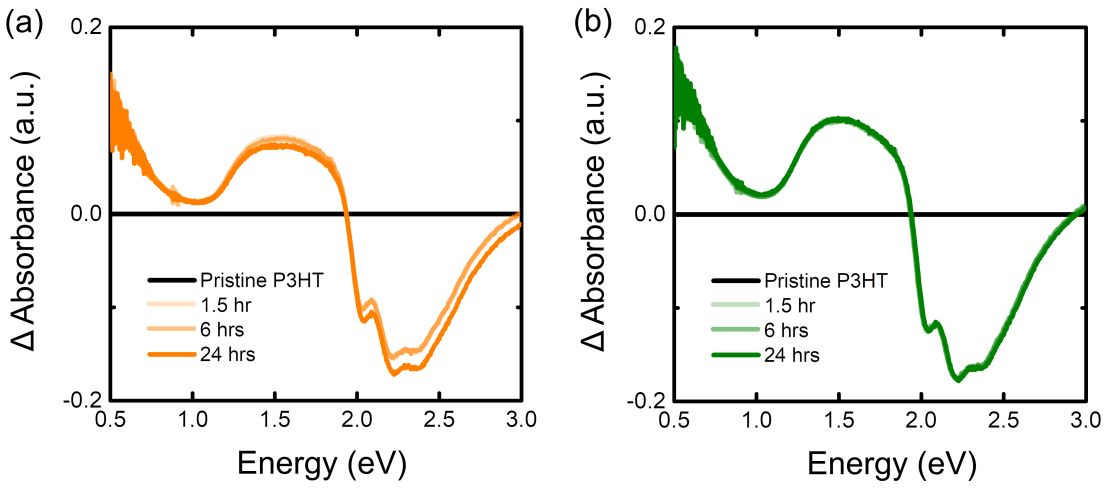

Fig S2. Delta absorbance of (black) pristine and (orange and green) doped P3HT film at each time point, with (a) 8.2% and (b)11.5% TFSI loaded pPTZ-EE.

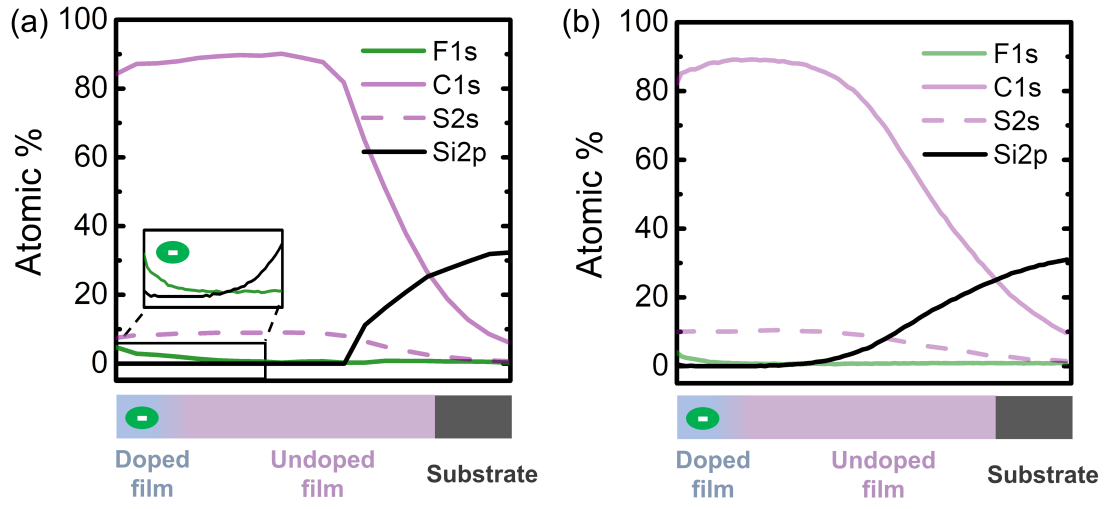

Fig S3. XPS spectra of surface doped P3HT layer with 11.5% TFSI. The pPTZ-EE$^{\bullet+}$-TFSI^{-} layer was spun-cast on the P3HT layer and the bilayer was left for (a) 30 min and (b) 24 hours.

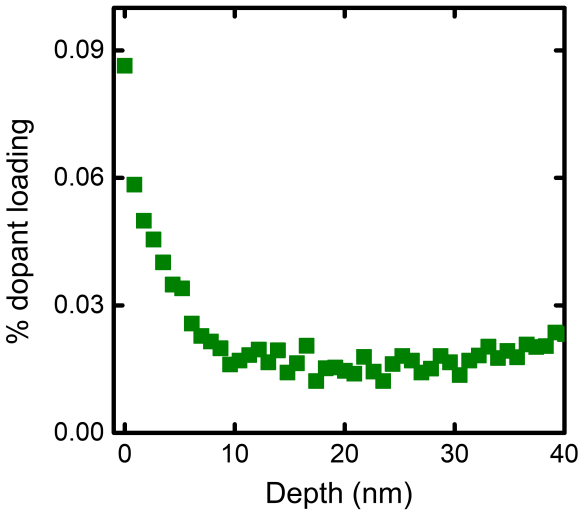

Fig S4. Relative % dopant loading per 3HT monomer unit with respective to film depth of surface doped P3HT layer with 11.5% TFSI.

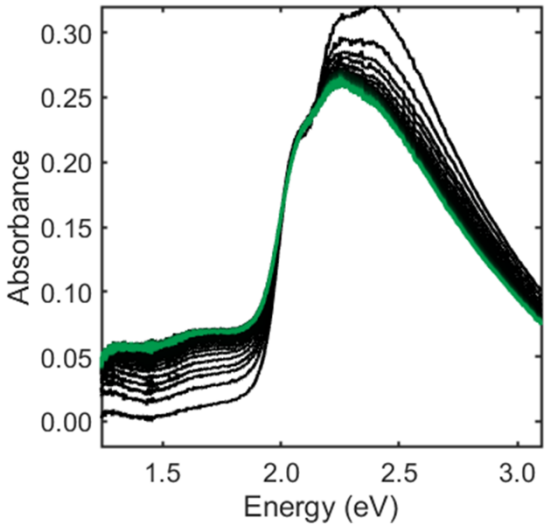

Fig S5. *In-situ* UV-vis absorption spectra of P3HT thin film in 0.1 mg/mL pPTZ-EE:4.7% TFSI solution. The green trace indicates the absorption spectra of P3HT thin film at 200 min.

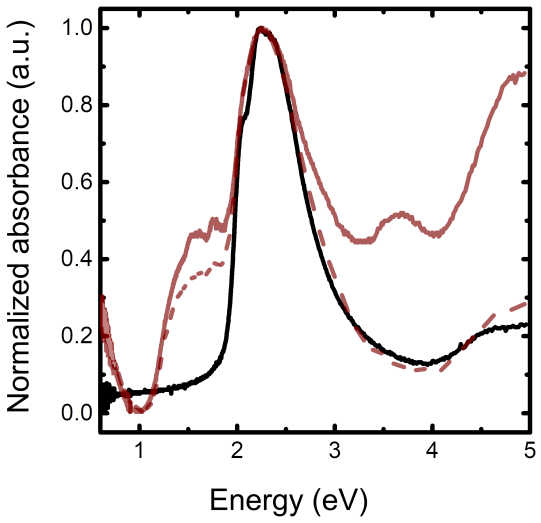

Fig S6. Normalized UV-vis-NIR spectra of pristine (black trace) and (wine trace) doped P3HT film with pPTZ- $EE^{\bullet+}$-TFSI 12.0% dopant loading. Dashed line indicates the absorption spectrum of doped P3HT after the DCM wash.

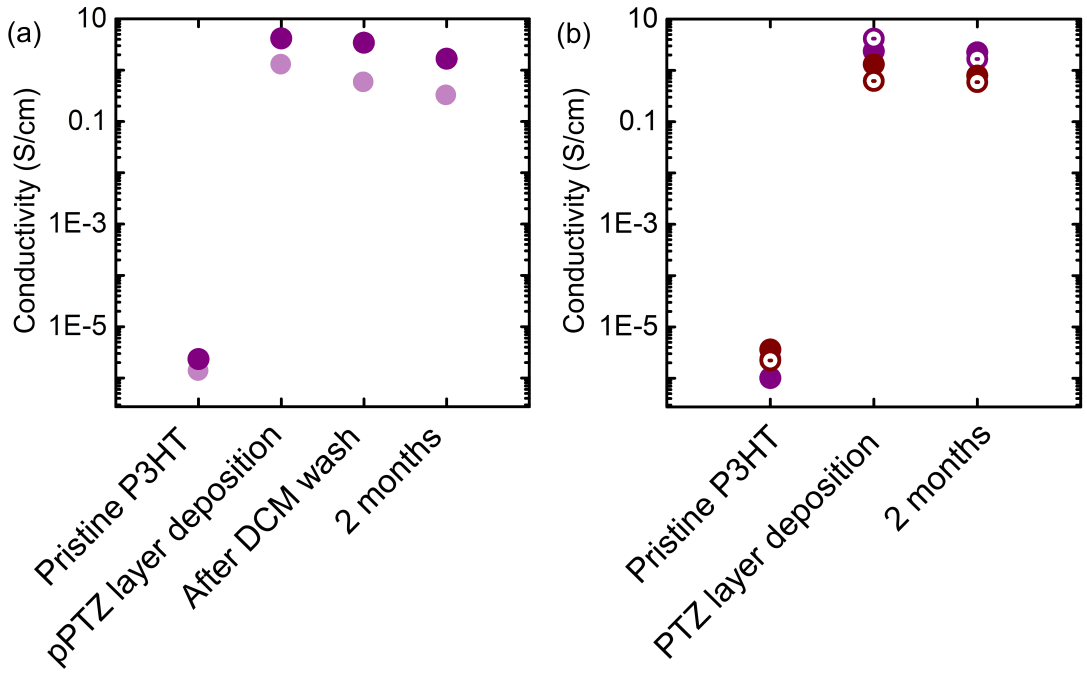

Fig S7. The changes in electrical conductivity of P3HT at various conditions with pPTZ-EE$^{\bullet+}$-TFSI^{-} and PTZ$^{\bullet+}$/TFSI^{-}. (Left) TFSI dopant ratio dependent plots on electrical conductivity, with 8.2% and 11.5% TFSI ratio. (Right) The effect of the top pPTZ-EE layer on the electrical conductivity changes. Purple and wine colors indicate bilayers formed with pPTZ- EE$^{\bullet+}$/TFSI *and* PTZ$^{\bullet+}$/TFSI, respectively. The intensity of purple color indicates the amount of TFSI loading in pPTZ-EE$^{\bullet+}$-TFSI^{-}. *Filled* and *empty* circles indicate the P3HT films that are stored *with* and *without* the PTZ/TFSI layers.

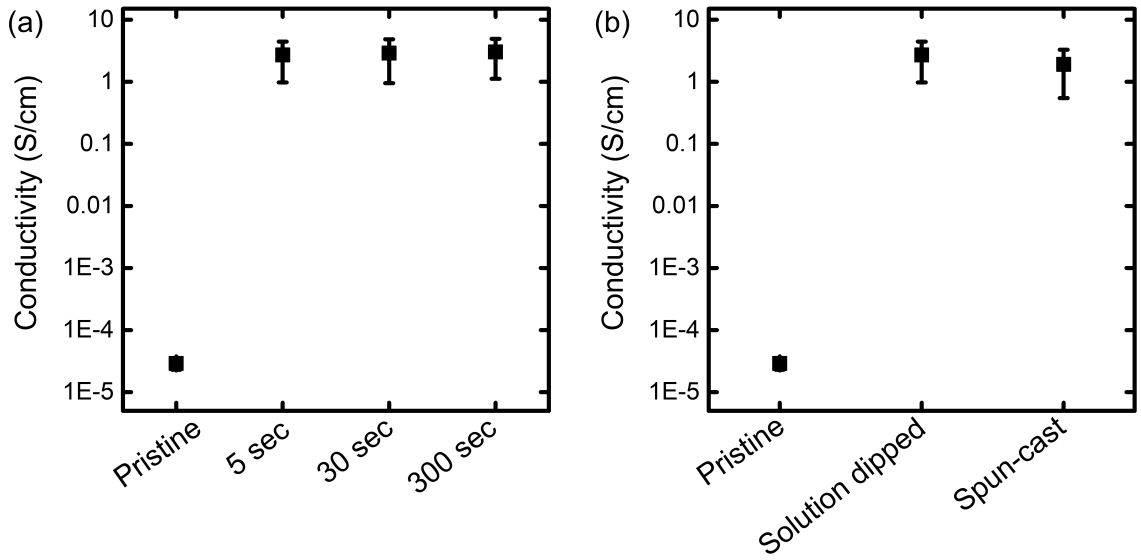

Fig S8. Electrical conductivity of P3HT film with 8.2% pPTZ-EE$^{\bullet+}$-TFSI^{-} solution dipping (a) at various time scale and (b) when comparing solution dipped and sequentially coated P3HT films.

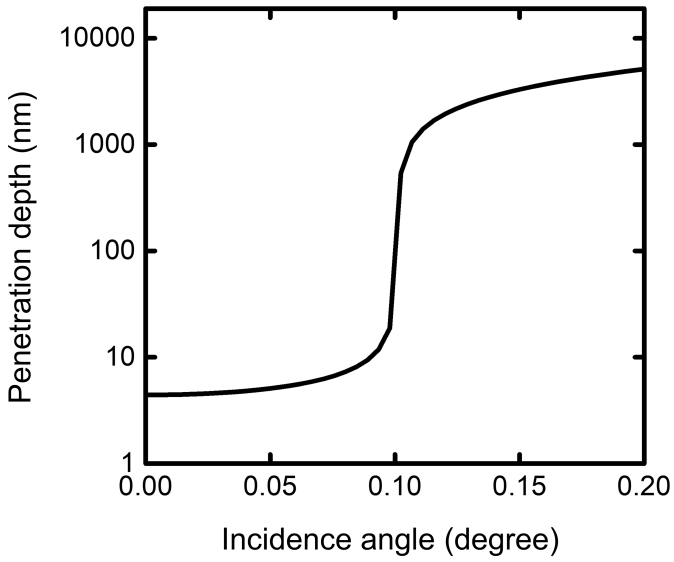

Fig S9. Penetration depth of x-ray beam into P3HT film with varying incidence angle.

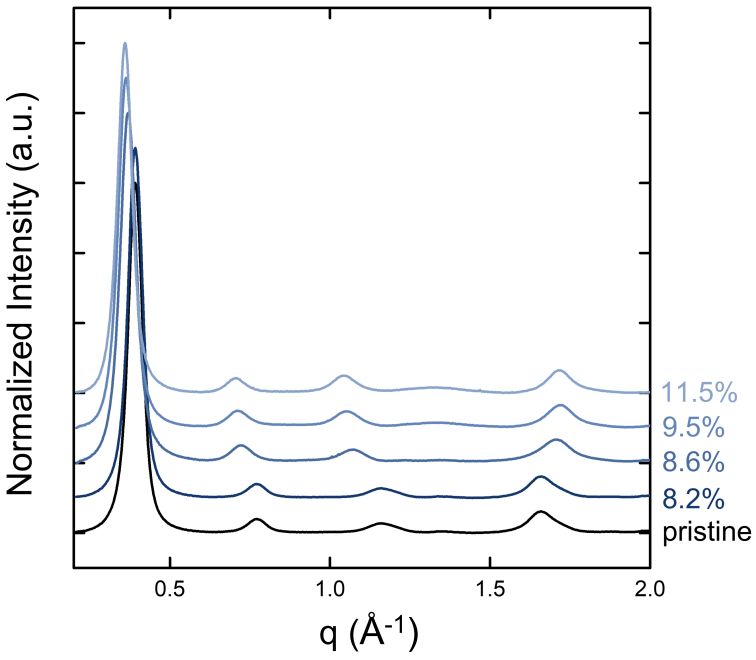

Fig S10. GIWAXS of pristine and doped P3HT thin films with various % $PTZ^{\bullet+}$:$TFSI^{-}$ loaded pPTZ-EE (incidence angle = 0.13°).

References:

1 S. Oh, A. Nikolaev, K. Tagami, T. Tran, D. Lee, S. Mukherjee, R. A. Segalman, S. Han, J. Read De Alaniz and M. L. Chabinyc, *ACS Appl Mater Interfaces*, 2021, **13**, 5319–5326.

2 C. J. Powell and A. Jablonski, *NIST Electron Inelastic-Mean-Free-Path Database - Version 1.2*, 2010, National Institute of Standards and Technology.

3 R. Escobar Galindo, R. Gago, D. Duday and C. Palacio, *Anal Bioanal Chem*, 2010, **396**, 2725–2740.

4 J. Hynynen, D. Kiefer, L. Yu, R. Kroon, R. Munir, A. Amassian, M. Kemerink and C. Müller, *Macromolecules*, 2017, **50**, 8140–8148.

5 H. Méndez, G. Heimel, S. Winkler, J. Frisch, A. Opitz, K. Sauer, B. Wegner, M. Oehzelt, C. Röthel, S. Duhm, D. Többens, N. Koch and I. Salzmann, *Nature Communications 2015 6:1*, 2015, **6**, 1–11.

6 G. Krauss, A. Hochgesang, J. Mohanraj and M. Thelakkat, *Macromol Rapid Commun*, 2021, **42**, 2100443.

7 N. G. Connelly and W. E. Geiger, *Chem Rev*, 1996, **96**, 877–910.

8 A. I. Hofmann, R. Kroon, S. Zokaei, E. Järsvall, C. Malacrida, S. Ludwigs, T. Biskup and C. Müller, *Adv Electron Mater*, 2020, **6**, 2000249.

9 M. Goel, M. Siegert, G. Krauss, J. Mohanraj, A. Hochgesang, D. C. Heinrich, M. Fried, J. Pflaum and M. Thelakkat, *Advanced Materials*, 2020, **32**, 2003596.

10 J. A. Kowalski, M. D. Casselman, A. P. Kaur, J. D. Milshtein, C. F. Elliott, S. Modekrutti, N. H. Attanayake, N. Zhang, S. R. Parkin, C. Risko, F. R. Brushett and S. A. Odom, *J Mater Chem A Mater*, 2017, **5**, 24371–24379.

11 Y. Sohn and J. T. Stuckless, *ChemPhysChem*, 2007, **8**, 1937–1942.

12 S. Janietz, D. D. C. Bradley, M. Grell, C. Giebeler, M. Inbasekaran and E. P. Woo, *Appl Phys Lett*, 1998, **73**, 2453.